IVYSPRING INTERNATIONAL PUBLISHER

Theranostics

2018; 8(1): 169-184. doi: 10.7150/thno.21234

Research Paper

Exosomes from human umbilical cord blood accelerate cutaneous wound healing through miR-21-3p-mediated promotion of angiogenesis and fibroblast function

Yin Hu[1, 4*], Shan-Shan Rao[1, 5*], Zhen-Xing Wang[1], Jia Cao[1], Yi-Juan Tan[1], Juan Luo[1], Hong-Ming Li[1, 4], Wei-She Zhang[6], Chun-Yuan Chen[1✉], Hui Xie[1, 2, 3, 4, 5✉]

1. Movement System Injury and Repair Research Center, Xiangya Hospital, Central South University, Changsha, Hunan, 410008, China;
2. Hunan Key Laboratory of Organ Injury, Aging and Regenerative Medicine, Changsha, Hunan, China;
3. Department of Sports Medicine, Xiangya Hospital, Central South University, Changsha, Hunan, 410008, China;
4. Department of Orthopedics, Xiangya Hospital, Central South University, Changsha, Hunan, 410008, China;
5. Department of Spine Surgery, Xiangya Hospital, Central South University, Changsha, Hunan, 410008, China;
6. Department of Obstetrics, Xiangya Hospital, Central South University, Changsha, Hunan, 410008, China.

* Yin Hu and Shan-Shan Rao contributed equally to this work.

✉ Corresponding authors: Hui Xie: huixie@csu.edu.cn; #88 Xiangya Road, Changsha, 410008, PR China; Tel: 86-0731-84327068; Chun-Yuan Chen: chency19@csu.edu.cn; #88 Xiangya Road, Changsha, 410008, PR China

Received: 2017.05.29; Accepted: 2017.10.02; Published: 2018.01.01

Abstract

The application of blood plasma for soft tissue wound healing is receiving much more attention recently. Exosomes are critical paracrine mediators that can be obtained from biological fluids including plasma and be able to induce regenerative effects by transferring bioactive molecules such as microRNAs (miRNAs). This study aimed to investigate the effects of exosomes from human umbilical cord blood plasma (UCB-Exos) on wound healing and to elucidate the underlying mechanism.

Methods: UCB-Exos were isolated by ultracentrifugation and subcutaneously injected into full-thickness skin wounds in mice. The efficacy of UCB-Exos on wound healing was evaluated by measuring wound closure rates, histological analysis and immunofluorescence examinations. *In vitro*, quantitative real-time PCR (qRT-PCR) analysis was performed to detect the expression levels of a class of miRNAs that have positive roles in regulating wound healing. The scratch wound assay, transwell assay and cell counting kit-8 analysis were conducted to assess the effects of UCB-Exos on migration and proliferation of human skin fibroblasts and endothelial cells. Tube formation assay was carried out to test the impact of UCB-Exos on angiogenic tube formation ability of endothelial cells. Meanwhile, by using specific RNA inhibitors or siRNAs, the roles of the candidate miRNA and its target genes in UCB-Exos-induced regulation of function of fibroblasts and endothelial cells were assessed.

Results: The local transplantation of UCB-Exos into mouse skin wounds resulted in accelerated re-epithelialization, reduced scar widths, and enhanced angiogenesis. *In vitro*, UCB-Exos could promote the proliferation and migration of fibroblasts, and enhance the angiogenic activities of endothelial cells. Notably, miR-21-3p was found to be highly enriched in UCB-Exos and served as a critical mediator in UCB-Exos -induced regulatory effects through inhibition of phosphatase and tensin homolog (PTEN) and sprouty homolog 1 (SPRY1).

Conclusion: Our results suggest that UCB-Exos are important effectors of plasma activity and can be used as a novel promising strategy for soft tissue wound healing.

Key words: exosomes, cord blood, wound healing, miR-21-3p.

Introduction

Skin and soft tissue injuries are a common occurrence following accidental traumas, such as bone fractures [1, 2]. The healing of skin/soft tissue wounds requires a well- orchestrated integration of cell migration and proliferation, collagen synthesis and deposition, angiogenesis, and wound remodeling [3]. In some pathological disorders, the normal wound healing process is disturbed and prolonged, which can lead to chronic non-healing wounds such as diabetic ulcers or pathological scarring such as keloid scars [3, 4]. Thus, shortening healing time and inhibiting scar formation after skin/soft tissue trauma represent urgent clinical needs. Although various therapeutic attempts have been made to promote wound healing, optimal treatment strategies are still being developed.

Over the past few years, stem cells have emerged as powerful tools to improve skin wound healing. Human umbilical cord blood (UCB) is an attractive source of transplantable stem cells for wound repair, and posesses several distinct advantages of no risk to donors, easy accessibility, and a low incidence of graft-versus-host disease [5, 6]. However, the direct use of stem cells for therapeutic purposes remains limited by many risk factors such as tumor formation, thrombosis, and unwanted immune responses [7-9]. Exosomes are 40-150 nm sized small membrane particles of endosomal origin that play crucial roles in intercellular communication by delivering miRNAs, mRNAs and proteins to recipient cells [10]. Exosomes exhibit stem cell-like pro-regenerative properties and direct treatment with them may avoid many adverse effects of stem cell transplantation therapy [11, 12]. Studies have reported that the local injection of exosomes secreted by human UCB-derived stem cells can promote skin cell proliferation and migration, angiogenesis, and wound closure in diabetic or burn wound animal models [11, 13], suggesting that exosomes-based therapy is a promising approach for wound healing. Except the stem cells, UCB also contain abundant exosomes [14]. Nevertheless, to date, few studies have directly utilized UCB to harvest exosomes for therapeutic uses.

In the present study, we isolated exosomes from human UCB-derived plasma (UCB-Exos) and explored the wound healing properties of UCB-Exos. The results showed that the local injection of UCB-Exos into full-thickness skin wounds in mice resulted in accelerated re-epithelialization, reduced scar widths, and enhanced new blood vessel formation. Moreover, we found that UCB-Exos could promote the proliferation and migration of fibroblasts, and enhance the angiogenic activities of endothelial cells *in vitro*. We also found that miR-21-3p was enriched in UCB-Exos and this miRNA was a key mediator in the UCB-Exos-induced regulation of function properties of fibroblasts and endothelial cells by inhibiting phosphatase and tensin homolog (PTEN) and sprouty homolog 1 (SPRY1). To the best of our knowledge, this study is the first to show the utility of UCB-Exos in soft tissue wound healing and elucidate the underlying mechanism.

Materials and Methods

Exosomes isolation from human UCB plasma

Human UCB samples (50-60 mL per sample) were obtained from umbilical veins after healthy neonatal delivery with permission from the infants' parents and the Institutional Review Board at Xiangya Hospital of Central South University. The whole blood was collected in a multiple system bag (Machopharma, Mouvax, France) containing citrate phosphate dextrose as anticoagulant. This mixture was transferred to 50 mL centrifuge tubes and centrifuged at 300 ×g for 10 min to collect the plasma. Subsequently, the plasma underwent a series of low-speed centrifugation steps (300 ×g for 10 min, 2,000 ×g for 10 min) to discard cell debris. Then, the supernatant was centrifuged at 10,000 ×g for 30 min followed by ultracentrifugation for 70 min at 100,000 ×g. The pelleted exosomes were washed twice with a large volume of PBS and centrifuged at 100,000 ×g for 70 min, then re-suspended in 15 mL of PBS. The exosomes suspension was filtered through a 0.22 μm filter (Merck-Millipore, Darmstadt, Germany) and centrifuged at 4000 ×g to about 200 μL by ultra-filtration in a 15 mL Amicon Ultra-15 Centrifugal Filter Unit (Millipore, Billerica MA, USA). All procedures were performed at 4 °C. Exosomes were stored at –80 °C or used for the downstream experiments. In total, UCB samples from three different healthy donors were collected successively to obtain UCB-Exos. At least three independent experiments were performed for verifying the effects of these exosomes on cultured fibroblasts and endothelial cells. Exosomes from one donor-derived UCB were used for assessing the efficacy of UCB-Exos in promoting wound healing *in vivo*.

Identification of UCB-Exos

The size distribution of UCB-Exos was measured by dynamic light scattering (DLS) with a Nanosizer™ instrument (Malvern Instruments, Malvern, UK) and the exosomes morphologies were observed with a Hitachi H-7650 transmission electron microscope (TEM) (Hitachi, Tokyo, Japan) as described previously in detail [11]. The characteristic surface marker proteins of exosomes were analyzed by flow cytometry. Briefly, exosomes were attached to 4 μm

aldehyde/sulfate latex beads (Invitrogen, Carlsbad, USA) and incubated with the primary antibodies mouse anti-human CD63 (Santa Cruz Biotechnology, Santa Cruz, USA, SC5275, 1:10) and rabbit anti-human TSG101 (ProteinTech, Chicago, USA, 14497-1-AP, 1:10). After washing with 2% BSA in PBS, the exosomes-bound beads were then incubated with Alexa Fluor® 488 conjugated goat anti-mouse IgG (Abcam, Cambridge, Britain, ab150117, 1:2000) or goat anti-rabbit IgG (Abcam, ab150077, 1:2000) secondary antibodies for 30 min. Negative controls using the respective isotype control primary antibodies + secondary antibodies or secondary antibodies alone were established. The isotype control primary antibodies of monoclonal mouse IgG (Cell Signaling Technology, Danvers, MA, #5415) and monoclonal rabbit IgG (Cell Signaling Technology, #3900) were used under the same concentrations and conditions. The beads un-coated with exosomes but incubated with the respective primary and secondary antibodies were served as blank. The beads were then washed and analyzed by flow cytometry using a Becton Dickinson FACSscan (San Jose, CA, USA). Results were analyzed with Flowjo software (Tree Star Inc, Ash-land, USA).

Mouse skin wound model and treatment

All procedures were approved by the Animal Research Committee of Xiangya Hospital of Central South University. 12-week-old male C57BL/6 mice (weighing 26–30 g) were used in this study. These mice were anesthetized by intraperitoneal (i.p.) administration of 50 mg/kg pentobarbital sodium (Sigma-Aldrich, St. Louis, MO, USA) before operation. After shaving the mice, two full-thickness excisional skin wounds (12 mm in diameter) were created on the dorsum. Twenty mice were randomly divided into two treatment groups, which were subcutaneously injected with UCB-Exos (200 μg dissolved in 100 μL PBS) or an equal volume of PBS around the wounds at 4 injection sites (25 μL per site). Eight days after operation, these mice were sacrificed and skin specimens were harvested. Skin samples were analyzed by histopathological methods.

Evaluation of wound closure and blood vessel regeneration

The wounds of each group were photographed at 0, 2, 5 and 8 days after surgery. All wounds were measured with a caliper ruler and the area of each wound was evaluated using Image-Pro Plus 6 software (Media Cybernetics, Bethesda, USA). The reduction of wound-size was calculated using the mathematical equation: wound-size reduction (%) = $(A_0 - A_t)/A_0 \times 100$, where A_0 is the initial wound area, and A_t is the wound area at day 2, 5 or 8 post-operation. To examine the formation of new blood vessels, the underside of skin at day 8 post-wounding was viewed and photographed.

Histological and immunofluorescence analysis

The collected specimens of mice containing the wound bed and surrounding healthy skin were processed for further investigation. The tissues were fixed in 4% paraformaldehyde solution, dehydrated with a series of graded ethanol and embedded in paraffin. Sections (10 μm thick) were stained with hematoxylin and eosin (H&E) and photographed under an optical microscope. The percentage of neo-epithelium was assessed basing on a method described previously [11]. Masson's trichrome was stained to evaluate the degree of collagen maturity. Immunofluorescence staining for CD31 was performed to estimate the extent of newly-formed capillaries during the wound-healing process. Briefly, skin samples at day 8 post-wounding were fixed in 4% paraformaldehyde, dehydrated in 30% sucrose solution and embedded in OCT. 10 μm thick sections were incubated with CD31 antibody (Abcam, Cambridge, Britain, ab28364, 1:50) overnight at 4 °C and then with the Cy3-conjugated secondary antibodies (Abcam, ab97075, 1:250) at room temperature for 1 h while avoiding light. Images were observed with a fluorescence microscope (Leica DMI6000B, Solms, Germany). To compare the number of blood vessels from different groups, six random fields per section near wound edges were counted by using Image-Pro Plus 6 software.

Cells culture

Human skin fibroblasts (HSFs; FuHeng Biology, Shanghai, China) were cultured in high-glucose Dulbecco's modified eagle medium (Gibco BRL, Grand Island, USA) with 10% FBS. Human microvascular endothelial cells (HMECs; Cell Bank of the Chinese Academy of Sciences, Shanghai, China) were cultured in MCDB131 medium (Gibco BRL) containing 10% FBS (Gibco BRL), 2 mM L-glutamine (Sigma-Aldrich), 1 μg/mL hydrocortisone (Sigma-Aldrich), and 10 ng/mL epidermal growth factor (Sigma-Aldrich). Cells were maintained at 37 °C with 5% CO_2 in a humidified environment.

Exosomes uptake by HSFs and HMECs

To determine UCB-Exos uptake by fibroblasts and endothelial cells, exosomes were labeled with a green fluorescent dye (PKH67; Sigma) as previously described [15] and then incubated with HSFs and HMECs at 37 °C for 3 h. The cells were then washed with PBS and fixed in 4% paraformaldehyde for 15 min. After washing with PBS, nuclei were stained

with DAPI (0.5 μg/mL; Invitrogen, Carlsbad, USA) and fluorescence microscopy was used to detect the green signals in HSFs and HMECs. To detect the miRNAs' transfer from exosomes to HSFs and HMECs, the recipient cells stimulated with exosomes for 3 h were harvested and the expression of miRNAs was analyzed by quantitative real-time PCR (qRT-PCR) analysis.

RNA interference

MiR-21-3p inhibitors and their negative control inhibitors were purchased from RiboBio (Guangzhou, China). Cells transfection was performed following the handbook from RiboBio. Briefly, the cells were cultured in 6-well culture plate and transfected with miR-21-3p inhibitor or the negative control inhibitor using Lipofectamine 2000 (Invitrogen), and cultured in complete medium containing 100 μg/mL UCB-Exos (200 μg/well) or an equal volume of PBS. After 24 h of incubation, the downstream experiments were performed.

To assess whether knocking down the expression of PTEN and SPRY1 can achieve similar effects as UCB-Exos on fibroblast function and endothelial angiogenesis, three PTEN siRNAs (siPTEN #1, 2 and 3) and three SPRY1 siRNAs (siSPRY1 #1, 2 and 3) obtained from RiboBio (Guangzhou, China) were respectively used to knockdown the expression of PTEN and SPRY1 in HSFs and HMECs. Briefly, cells were transfected with siPTEN, siSPRY1 or the universal negative control siRNA (Con siRNA) using Lipofectamine 2000 (Invitrogen) according to the instructions of the manufacturers. 24 h later, the inhibitory efficiency of these siRNAs was verified by qRT-PCR and the most effective siRNAs were used for the downstream functional experiments. The same experiments were performed on cells treated with UCB-Exos (100 μg/mL) or an equal volume of PBS.

Migration assay

For the scratch wound assay, 2×10^5 cells/well (three replicates per group) were plated into a 12-well plate and incubated to reach confluence. The monolayer was scratched using a tip and washed with serum-free medium to remove detached cells. Then the cells were cultured in complete medium supplemented with or without UCB-Exos (100 μg/well) and miR-21-3p inhibitor. HSFs were photographed at 0 h, 12 h and/or 24 h later; HMECs were photographed at 0 h, 6 h and/or 12 h post-wounding. The closure area of wound was calculated as follows: migration area (%) = $(A_0 - An)/A_0 \times 100$, where A_0 represents the area of initial wound area, An represents the remaining area of wound at the metering point.

For the transwell assay, 1×10^4 cells/well (three replicates per group) were suspended in low serum (5% FBS) medium and seeded into the upper chamber of transwell 24-well plates (Corning, Corning, NY, USA) with 8 μm pore filters. Then the lower chamber was added with complete medium (containing 10% FBS) supplemented with or without UCB-Exos (50 μg/well) and miR-21-3p inhibitor. After 12 h, the cells attached on the upper surface of the filter membranes were cleaned and migrated cells of the lower surface were stained with 0.5% crystal violet for several minutes. The level of migration was observed under an optical microscope (Leica DMI6000B, Germany).

Proliferation assay

The effects of UCB-Exos on cell proliferation were determined by a cell counting kit-8 assay (CCK-8; Dojindo, Kyushu Island, Japan). Briefly, 5×10^3 cells/well (four replicates per group) were seeded into 96-well plates and cultured in medium supplemented with or without UCB-Exos (10 μg/well) and miR-21-3p inhibitor. A group without cells served as the blank. Day 1, 2, 3, 4, and 5, CCK-8 solution (10 μL) and 100 μL of fresh culture medium was added to each well and incubated at 37 °C for 1 h. The absorbance was observed at 450 nm by using a microplate reader (Bio-Rad 680, Bio-Rad, Hercules, CA, USA). The survival/proliferation of cells was represented through the absorbance of the test wells minus the optical density of the blank wells.

Tube formation assay

Growth Factor Reduced Matrigel (BD Biosciences, New Jersey, USA) was plated in 96-well plates and incubated at 37 °C to gel for 30 min. Then, 2×10^4 /well HMECs (three replicates per group) were added on polymerized Matrigel in plates treated with or without UCB-Exos (10 μg/well) and miR-21-3p inhibitor. After incubation at 37 °C for 6 h, tube formation was observed by an inverted microscope (Leica DMI6000B, Germany). The total branching points and total tube length were measured by Image-Pro Plus 6 software.

qRT-PCR analysis

Total RNA was extracted from cultured cells using Trizol Reagent (Invitrogen). For mRNA detection, cDNA was synthesized from 1 μg of total RNA by using a Revert Aid first-strand cDNA synthesis kit (Fermentas, Life Sciences, Canada). Then, qRT-PCR analysis was performed with SYBR Premix ExTaq™II in an ABI PRISM® 7900HT System (Takara Biotechnology, Japan). The relative standard curve method ($2^{-\Delta\Delta CT}$) was used to determine the relative mRNA expression, using GAPDH as the

reference. The PCR primers used in this study were as follows: hsa-PTEN: forward, 5'-AGGGACGAACTGG TGTAATGA-3', and reverse, 5'-CTGGTCCTTACTTC CCCATAGAA-3'; hsa-SPRY1: forward, 5'-CCCACTG CTGACACAAGGAG-3', and reverse, 5'-ACACTAGC CCATCCACATTTTG-3'; hsa-GAPDH: forward, 5′-ATCCCATCACCATCTTCC-3′, and reverse, 5′-GAGTCCTTCCACGATACCA-3′. For miRNA analysis, exosomal miRNAs were isolated by using the SeraMir Exosome RNA Purification Kit (System Biosciences, Mountain View, USA), and cDNA for miRNAs was synthesized using the TaqMan microRNA assay kit (Applied Biosystems, Foster City, USA) as described by the manufacturer's protocol. The qRT-PCR reaction was performed using FastStart Universal SYBR Green Master Mix (Roche, Indianapolis, USA) with the miRNA-specific forward primer (Sangon Biotech, Shanghai, China) and the universal reverse primer provided by the TaqMan microRNA assay kit. U6 small nuclear RNA was used to normalize the results.

Western blotting

Protein extracts were separated by sodium dodecyl sulfate-polyacrylamide gel electrophoresis (SDS-PAGE) and transferred to polyvinylidene fluoride membranes (Immobilon P, Millipore, Billerica, USA). Blots were blocked with 5% milk in Tris-buffered saline containing 0.1% Tween-20 for 1 h at room temperature. The membranes were incubated with primary antibodies at 4 °C overnight, followed by incubation with the horseradish peroxidase-conjugated secondary antibodies at 37 °C for 1 h. The antibodies including anti-phosphorylate Akt (p-Akt; #9271, 1:1000), anti-Akt (#9272, 1:1000), anti-p-Erk1/2 (#4370, 1:2000), anti-Erk1/2 (#4695, 1:1000), anti-β-actin (#3700, 1:1000), horseradish peroxidase conjugated anti-rabbit IgG (#7074, 1:5000) and anti-mouse IgG (#7076, 1:5000) were obtained from Cell Signaling Technology (Danvers, MA, USA). The immunoreactive bands were visualized using enhanced chemiluminescence reagent (Thermo Fisher Scientific, Waltham, USA) and imaged by the ChemiDoc XRS Plus luminescent image analyser (Bio-Rad). Densitometric quantification of band intensity from four independent experiments was carried out with Image-Pro Plus 6.0 software and the relative expression level of target protein was normalized to the band intensity of β-actin.

Statistical analysis

All experiments were performed with at least three replicates per group and the *in vitro* experiments were repeated at least three times. Data are representative of these experiments and are shown as means ± standard deviation (SD). Means of multiple groups were compared with one-way analysis of variance (ANOVA). Independent-sample *t* test was used to compare means between two different groups. Statistical analysis was conducted using GraphPad Prism software and $P < 0.05$ was considered statistically significant.

Results

Characterization of UCB-Exos

DLS analysis, TEM and flow cytometric analysis were performed to identify the purified nanoparticles derived from UCB. DLS measurement showed that the diameters of these particles predominantly ranged from 30 nm to 100 nm (**Fig. 1A**), which was consistent with the previously reported exosomes size distributions [10]. TEM revealed that UCB-Exos exhibited a cup- or sphere-shaped morphology (**Fig. 1B**), similar to previously described exosomes [10]. The identity of these particles was further confirmed as exosomes by flow cytometric analysis, which showed the presence of exosomal surface markers including CD63 and TSG101 (**Fig. 1C**). All these data suggested that these nanoparticles were actually exosomes.

UCB-Exos promote cutaneous wound healing in mice

To evaluate the effects of UCB-Exos on wound healing, full-thickness cutaneous wounds were created on the back of mice, followed by subcutaneous injection of UCB-Exos or an equal volume of exosomes diluents (PBS). Digital photographs showed the progress in closure of wounds receiving different treatments. As shown in **Fig. 2A-B**, wound closure of the exosomes-treated mice was accelerated, illustrated by smaller wound areas measured at day 2, 5, and 8 post-wounding when compared with the PBS-treated control group. In particular, the wounds treated with UCB-Exos had almost closed at day 8 whereas large scar areas remained detectable in the control wounds. H&E staining revealed that the exosomes-treated wounds showed longer neo-epidermis and dermis with regenerated hair follicles and fat cells than that of the PBS-treated wounds at day 8 post-wounding (**Fig. 2C**). Quantification of the rate of re-epithelialization and scar width further confirmed that exosomes transplantation enhanced epidermal regeneration and reduced scar formation of wounds (**Fig. 2D**). Masson's staining showed larger amounts of wavy collagen fibers in the wounds treated with exosomes compared with the controls (**Fig. 2E**). These data indicate that UCB-Exos treatment results in the

acceleration of the wound healing process in mice.

UCB-Exos enhance angiogenesis in the wound sites of mice

We then asked whether the transplantation of UCB-Exos could enhance angiogenesis in the wound area. As shown in **Fig. 3A**, larger numbers of newly formed blood vessels were observed in the wounds treated with UCB-Exos at day 8 post-wounding compared with the control wounds. Immunofluorescence staining for CD31 was also performed to detect the extent of blood vessel formation in the wound sites. As shown in **Fig. 3B**, the blood vessels were rarely observed in the PBS-treated wounds, whereas abundant blood vessels appeared in the wounds treated with exosomes. Quantification of the density of new blood vessels, defined as the number of CD31 positively stained cells per mm^2, verified the increase of the number of blood vessels induced by exosomes (**Fig. 3C**). Our data suggest that UCB-Exos transplantation augment the angiogenic responses of the wound sites in mice.

Retention of UCB-Exos in skin tissues

We also tested the retention of the administered UCB-Exos in skin tissues. As detected by fluorescence microscopy, plenty of PKH67-labeled UCB-Exos were observed in the perinuclear region of skin cells at 3 h after injection, but the signal decreased at 24 h after injection. At 2 d after injection, UCB-Exos were found at a significantly lower density in skin tissues. On day 5 and day 8, no fluorescent signal was detected (**Fig. S1A**). Quantitative analysis of the numbers of skin cells that took up the PKH67-labeled exosomes at indicated times further confirmed the time-dependent decrease of injected exosomes around the wound sites (**Fig. S1B**). The results suggest that the transplanted UCB-Exos provide time-dependent decrease of stimuli to the resident skin cells.

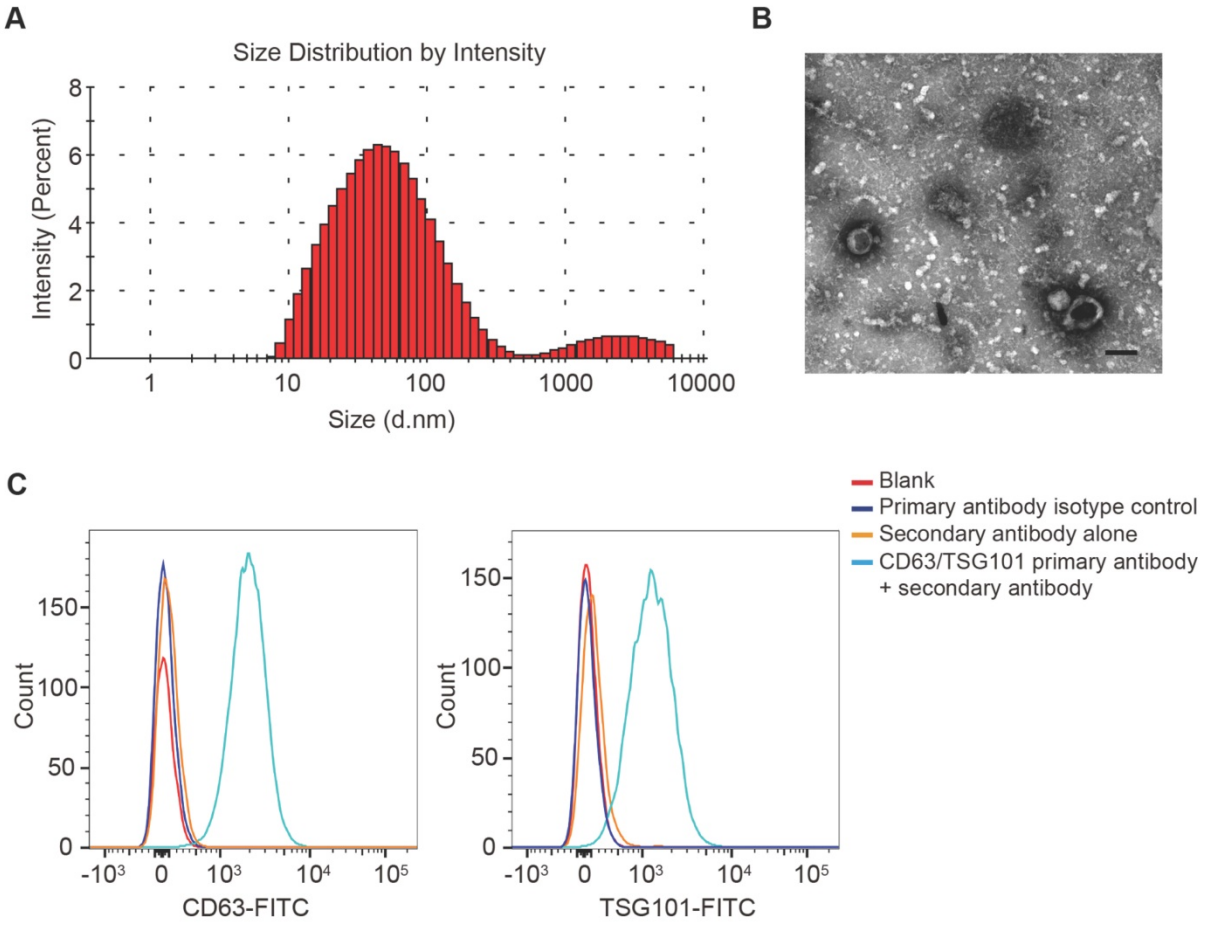

Figure 1. Characterization of UCB-Exos. (A) Particle size distribution of UCB-Exos measured by DLS analysis. **(B)** Morphology of UCB-Exos observed by TEM. Scale bar: 50 nm. **(C)** Representative flow cytometry histograms showing the presence of exosomal surface markers CD63 and TSG101 on UCB-Exos-bound beads. Negative controls: isotype control primary antibody + secondary antibody or secondary antibody only. The beads un-coated with exosomes but incubated with the respective primary and secondary antibodies served as blank.

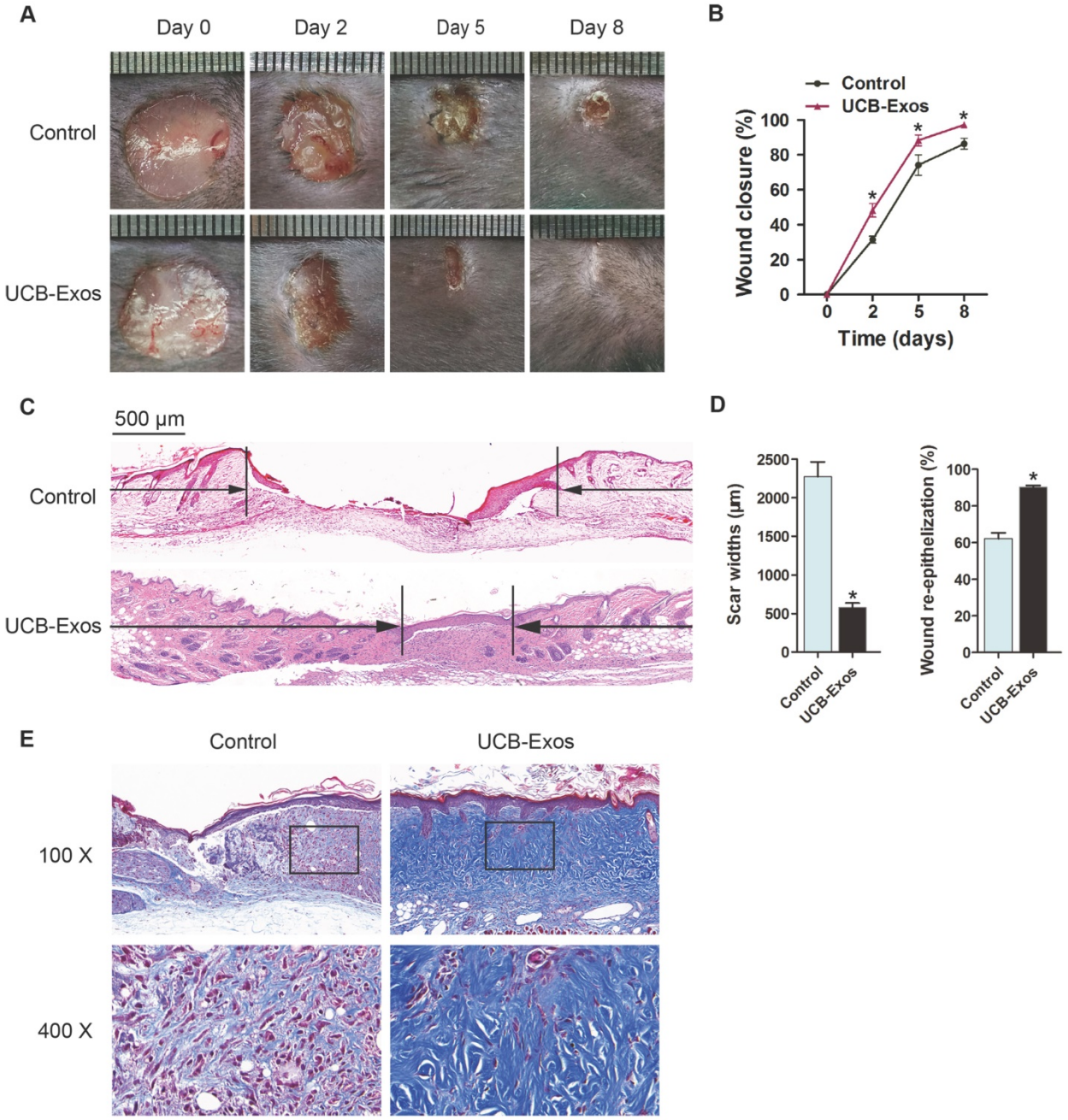

Figure 2. UCB-Exos transplantation was beneficial for cutaneous wound healing in mice. (A) Gross view of wounds treated with UCB-Exos or PBS at day 2, 5 and 8 post-wounding. **(B)** The rate of wound-closure in wounds receiving different treatments. n = 10 per group. **(C)** H&E staining of wound sections treated with UCB-Exos or PBS at 8 days after operation. The black arrows indicate the edges of the scar. Scale bar: 500 μm. **(D)** Quantification of the scar widths and the extent of re-epithelialization. n = 3 per group. **(E)** Masson's trichrome staining of wound sections treated with UCB-Exos or PBS. *P < 0.05 compared with the PBS group (control).

Detection of miRNAs in UCB-Exos

To explore the functional molecules that mediate the pro-wound healing effects of UCB-Exos, quantitative real-time PCR (qRT-PCR) analysis was performed to detect the expression levels of a class of miRNAs (including miR-21, miR-214, miR-126, miR-27b, miR-125b and miR-19b) that have positive roles in regulating fibroblast function and/or angiogenesis in UCB-Exos. The result showed that miR-21-3p, but not miR-21-5p, was the most highly expressed miRNA among these detected miRNAs (**Fig. 4A**). Studies have indicated that miR-21 can not only promote fibroblasts proliferation, migration and collagen synthesis [16, 17], but also enhance the angiogenic activities of endothelial cells [18], both of which are beneficial for wound healing. Thus, we focused on exosomal miR-21-3p for further investigation.

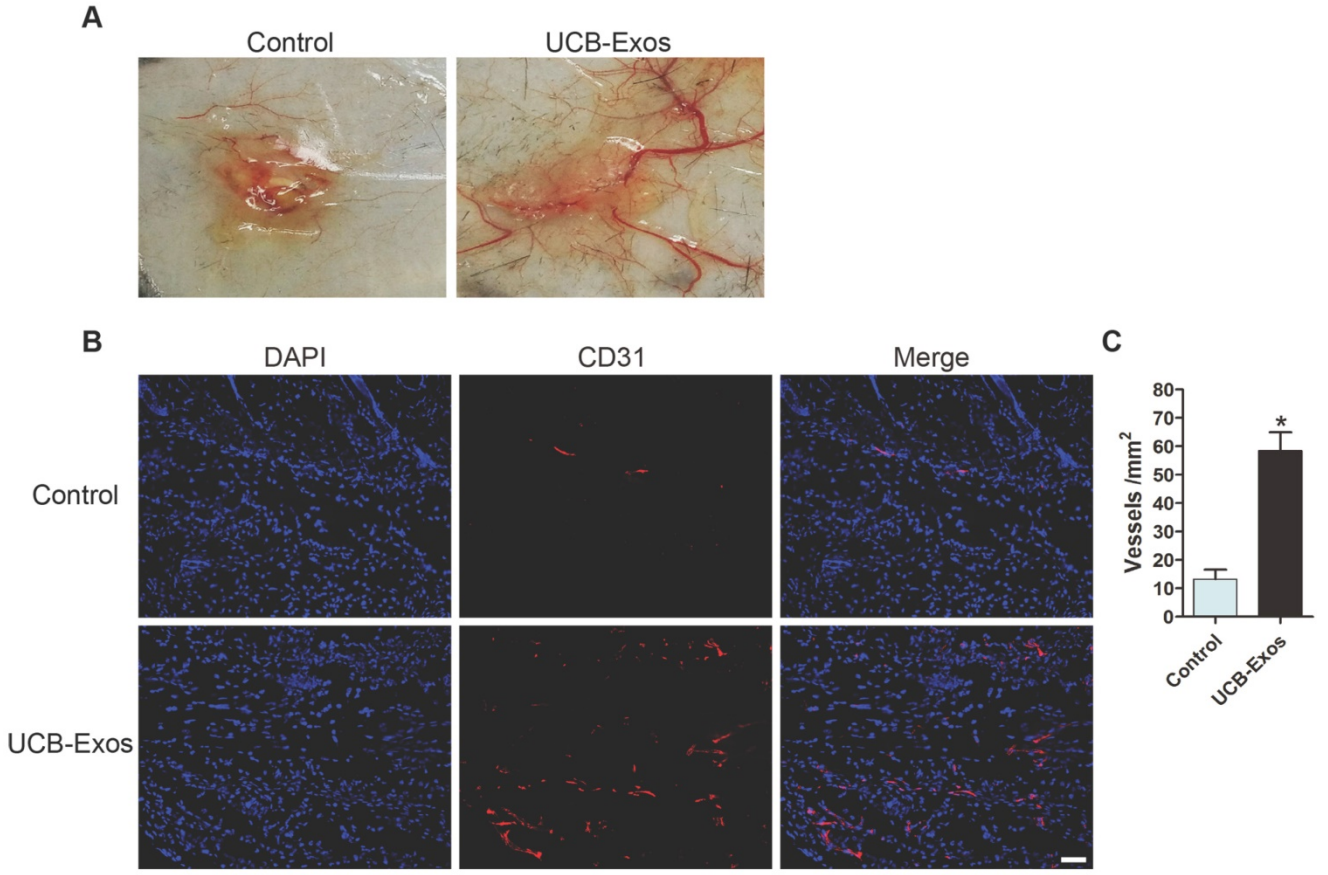

Figure 3. UCB-Exos enhance angiogenesis in the wound sites of mice. (A) Gross view of wounds receiving different treatments at day 8 post-wounding from the undersurface. Newly formed blood vessels were detected in the wound sites. **(B)** CD31 immunofluorescence staining of wound sections treated with UCB-Exos or PBS. Scale bar: 50 μm. **(C)** Quantitative analysis of the number of blood vessels in (B). n = 3 per group. *$P < 0.05$ compared with the PBS group (control).

UCB-Exos shuttle miR-21-3p into fibroblasts and endothelial cells

Next, we determined whether UCB-Exos could be internalized into fibroblasts and endothelial cells, a prerequisite for subsequent exosomal miRNA transfer. UCB-Exos were labeled by the green fluorescent dye (PKH67) and then were incubated with human skin fibroblasts (HSFs) and human microvascular endothelial cells (HMECs). After 3 h, recipient cells were washed to remove unbound exosomes and fixed, and DNA was stained with DAPI. Fluorescence microscopy analysis revealed that the PKH67-labeled exosomes had been transferred to perinuclear region of HSFs and HMECs (**Fig. 4B**).

To verify the transfer of miR-21-3p into recipient cells, HSFs and HMECs were treated with UCB-Exos and the cells were harvested for qRT-PCR analysis. As shown in **Fig. 4C-D**, miR-21-3p levels in HSFs and HMECs were remarkably increased after the cells were stimulated with UCB-Exos for 3 h. However, the levels of its target genes, including PTEN and SPRY1, were markedly reduced after treatment with exosomes for 24 h (**Fig. 4E-F**). The results indicate that miR-21-3p can be transferred into target cells to regulate gene expression.

UCB-Exos promote fibroblast proliferation and migration via transferring miR-21-3p

To assess the effects of UCB-Exos on fibroblasts, HSFs were treated with UCB-Exos or an equal volume of PBS for a series of *in vitro* functional assays. A scratch wound assay was applied to measure the effect of UCB-Exos on the migration of HSFs. The result showed that exosomes treatment markedly enhanced the motility of HSFs, as determined by the migration area (**Fig. 5A-B**). The pro-migratory ability of UCB-Exos was further confirmed by the transwell assay (**Fig. 5C-D**), which is another widely used method for evaluating the migration of cells. To verify the role of miR-21-3p in the exosomes-induced regulation of fibroblasts, HSFs stimulated with exosomes were additionally treated with a specific inhibitor targeting miR-21-3p. As illustrated in **Fig. 5A-D**, the pro-migratory effect of UCB-Exos was attenuated, but not totally abolished, in the UCB-Exos+miR-21-3p inhibitor group. The proliferation of HSFs was quantified by CCK-8

analysis. The result revealed that exosomes stimulation resulted in a significant increase in HSFs proliferation, but the effect was reduced by the miR-21-3p inhibitor (**Fig. 5E**). The expression of PTEN and SPRY1 in HSFs receiving different treatments was also evaluated. As shown in **Fig. 5F**, inhibition of miR-21-3p markedly reversed the UCB-Exos-induced reduction of PTEN and SPRY1 in HSFs. All these data suggest that UCB-Exos can enhance fibroblast function by targeting PTEN and SPRY1 through miR-21-3p.

The activation of PI3K/Akt and ERK1/2 signaling in fibroblasts in response to UCB-Exos stimulation

Studies have shown that miR-21 can target PTEN and SPRY1 in fibroblasts to induce the activation of PI3K/Akt and ERK1/2 pathways [19, 20]. To detect whether UCB-Exos could deliver miR-21-3p to activate these signaling pathways, western blotting was carried out to assess the protein levels of Akt, p-Akt, Erk1/2 and p-Erk1/2 in HSFs following treatment with UCB-Exos or PBS under normal or miR-21 inhibition conditions for 24 h. The western blotting images and the quantitative data of the relative band intensites revealed that UCB-Exos induced significant increases in the phosphorylation of Akt and Erk1/2, but the miR-21-3p inhibitor markedly decreased their up-regulation induced by exosomes (**Fig. 5G-H**). Thus, the activation of PI3K/Akt and ERK1/2 pathways may be the underlying mechanism by which miR-21-3p-containing UCB-Exos enhance fibroblast function.

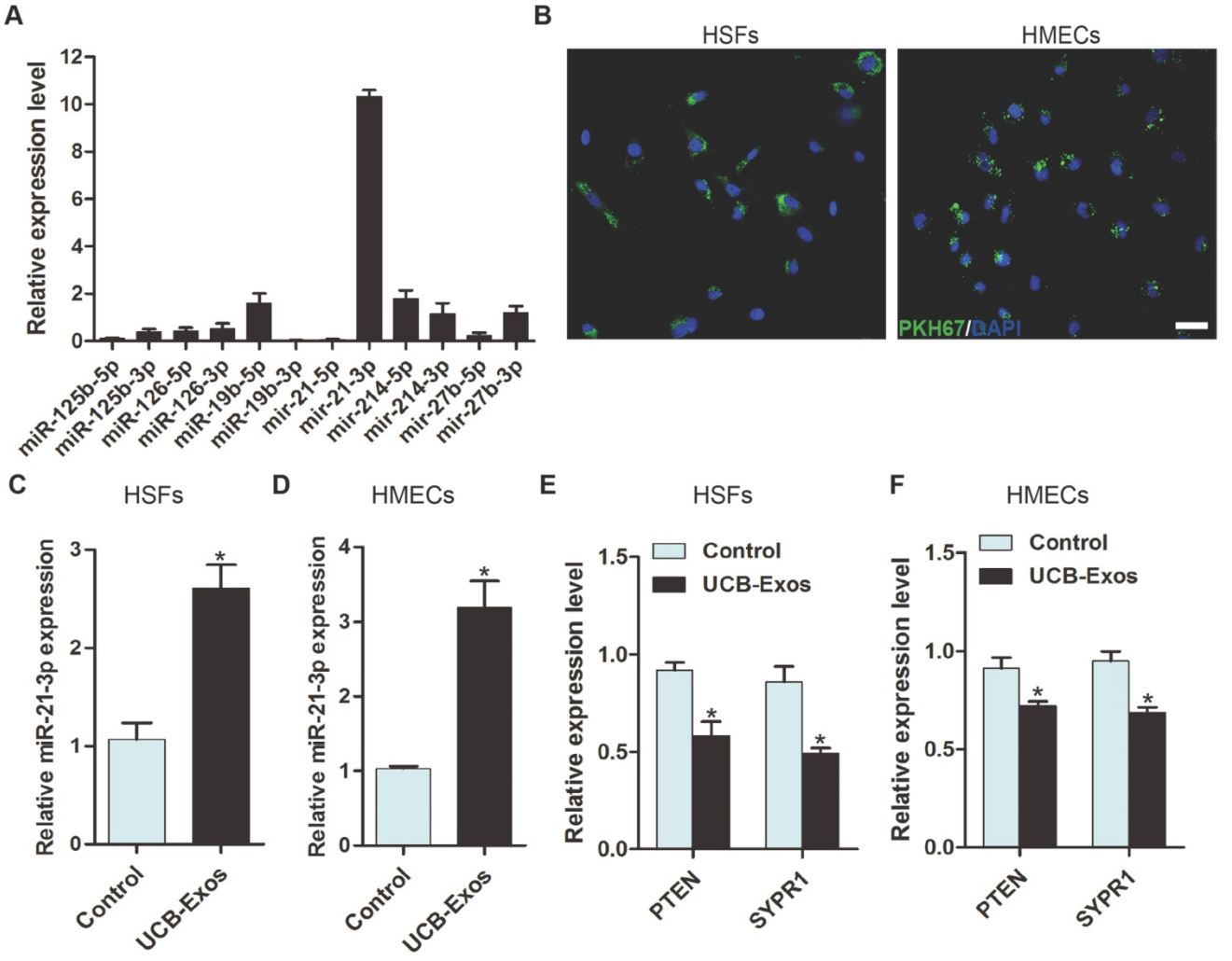

Figure 4. UCB-Exos deliver miR-21-3p into fibroblasts and endothelial cells. (A) Detection of the expression of the indicated miRNAs by qRT-PCR analysis. n = 3. **(B)** Fluorescence microscopy analysis of PKH67-labeled UCB-Exos internalization by HSFs and HMECs. The green-labeled exosomes were visible in the perinuclear region of recipient cells. Scale bar: 50 μm. **(C-D)** HSFs and HMECs incubated with UCB-Exos for 3 h showed higher expression levels of miR-21-3p than controls did. n = 3 per group. Incubation with UCB-Exos for 24 h reduced the expression of PTEN and SPRY1 in HSFs **(E)** and HMECs **(F)**. n = 3 per group. UCB-Exos were used at a concentration of 100 μg/mL. *$P < 0.05$ compared with the PBS group (control).

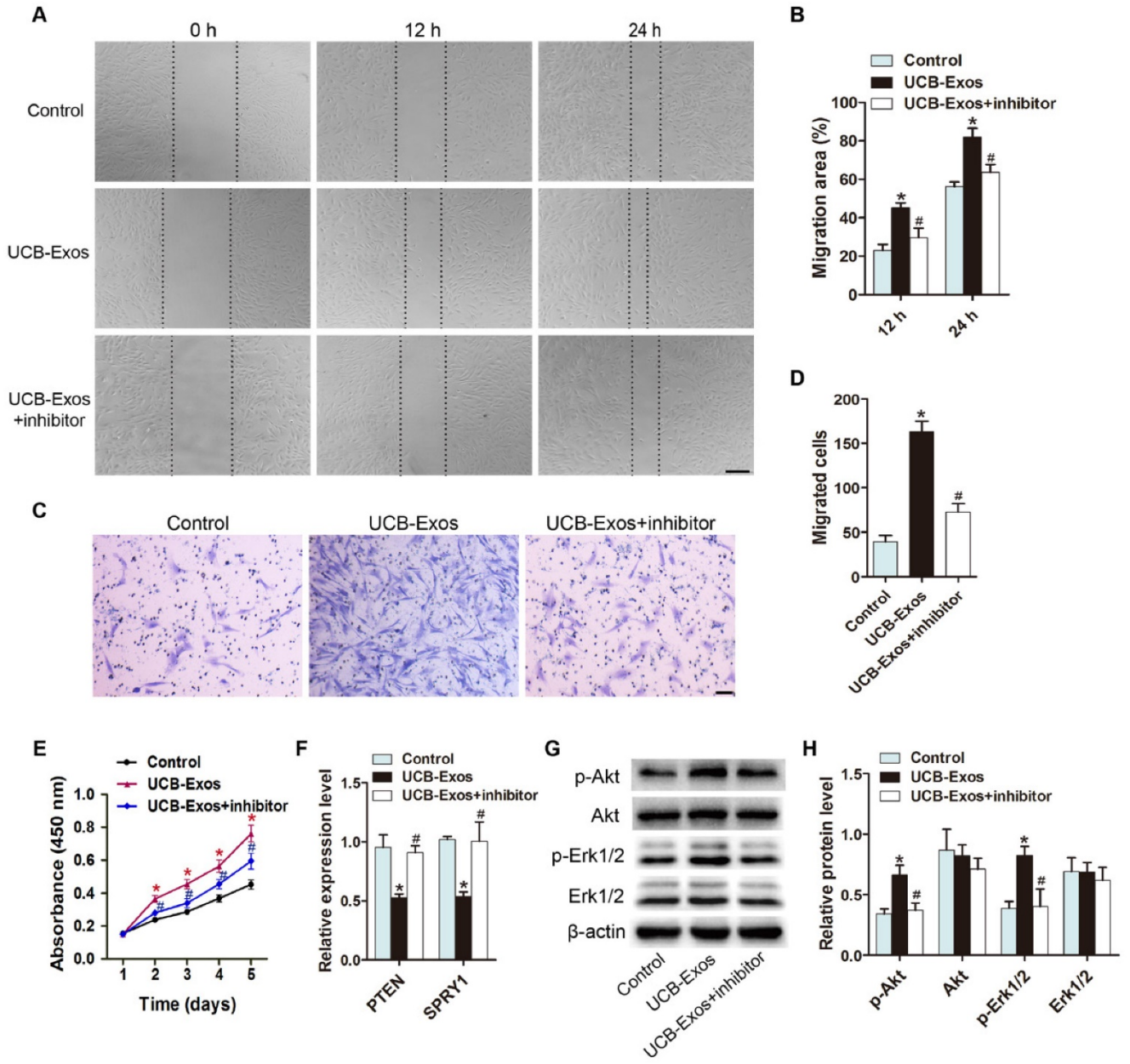

Figure 5. UCB-Exos promote the proliferation and migration of fibroblasts via transferring miR-21-3p. (A) UCB-Exos promoted HSFs migration as analyzed by scratch wound assay, but this effect was reduced by miR-21-3p inhibitor. Scale bar: 250 μm. **(B)** Quantitative analysis of the migration rates in (A). n = 3 per group. **(C)** The migratory ability of HSFs receiving different treatments was further confirmed by the transwell assay. Scale bar: 100 μm. **(D)** Quantitative analysis of the migrated cells in (C). n = 3 per group. **(E)** CCK-8 assay showed that UCB-Exos promoted HSFs proliferation, whereas this effect was attenuated by miR-21-3p inhibition. n = 4 per group. **(F)** UCB-Exos reduced the expression of PTEN and SPRY1 in HSFs, but their down-regulation was reversed by the miR-21-3p inhibitor. n = 3 per group. **(G)** UCB-Exos incubation enhanced the protein levels of p-Akt and p-Erk1/2 in HSFs, whereas this effect was reduced in the miR-21-3p co-treatment group. **(H)** Densitometric quantification of the relative band intensity in (G). n = 4 per group. **P* < 0.05 compared with the control group, # *P* < 0.05 compared with the UCB-Exos (100 μg/mL) group.

Inhibition of PTEN and SPRY1 induces UCB-Exos-like positive effects on fibroblast function

We next asked whether knocking down the expression of miR-21 target genes, PTEN and SPRY1, could achieve the similar positive effects like UCB-Exos on fibroblast function. Three PTEN siRNAs (siPTEN #1, 2 and 3) and three SPRY1 siRNAs (siSPRY1 #1, 2 and 3) were used to downregulate the expression of PTEN and SPRY1 in HSFs, respectively. The inhibitory efficiency of these siRNAs was verified by qRT-PCR (**Fig. 6A**) and the most effective siRNAs (siPTEN #1 and siSPRY1 #2) were used for the following functional assays. The results of scratch wound assay (**Fig. 6B-C**) and CCK-8 assay (**Fig. 6D**) respectively revealed that inhibition of PTEN and SPRY1 significantly enhanced the motility and proliferation of HSFs. All these effects on HSFs

induced by siPTEN #1 and siSPRY1 #2 were similar to those observed following exposure to UCB-Exos (**Fig. 6B-D**), which further indicates that the positive effects of UCB-Exos on fibroblast function are mediated by miR-21-3p-induced inhibition of PTEN and SPRY1.

MiR-21-3p mediates the pro-angiogenic effects of UCB-Exos on endothelial cells by inhibiting PTEN and SPRY1

We then investigated whether UCB-Exos could influence the angiogenic responses of endothelial cells and the role of miR-21-3p in these processes. The scratch wound assay and the transwell assay indicated that UCB-Exos remarkably up-regulated the migration of HMECs. However, miR-21-3p inhibition impaired the pro-migratory effect of UCB-Exos (**Fig. 7A-D**). CCK-8 assay showed that UCB-Exos enhanced the proliferative activity of HMECs, whereas co-treatment with the miR-21-3p inhibitor lowered the exosomes-induced proliferation of HMECs (**Fig. 7E**). The tube formation assay on Matrigel is an *in vitro* model of angiogenesis. The total tube length and total branching points at the indicated time were measured to quantify the ability of HMECs to form tubes. As shown in **Fig. 7F-G**, all the indicators were increased in the exosomes-treated HMECs. When the cells were transfected with the miR-21-3p inhibitor, the exosomes-induced tube formation was reduced. The result of qRT-PCR analysis showed that the down-regulation of PTEN and SPRY1 induced by UCB-Exos was attenuated by miR-21-3p inhibition (**Fig. 7H**). We also detected the activity of PI3K/Akt and ERK1/2 signaling in HMECs, the downstream pathways that can be activated by miR-21 and thereby enhance angiogenesis [21]. As evidenced by the western blotting images and the quantitative data, UCB-Exos incubation enhanced the protein levels of p-Akt and p-Erk1/2 in HMECs, whereas their up-regulation was inhibited in the miR-21-3p inhibitor co-treatment group (**Fig. 7I-J**).

The angiogenic activities of HMECs were also assessed after PTEN and SPRY1 interference by using specific siRNAs. Downregulation of PTEN and SPRY1 was verified by qRT-PCR (**Fig. 8A**). The PTEN- and SPRY1-silenced cells by siPTEN #1 and siSPRY1 #1 were selected for the downstream experiments. As evidenced by scratch wound assay (**Fig. 8B-C**), tube formation assay (**Fig. 8D-E**) and CCK-8 assay (**Fig. 8F**), the migration, angiogenic tubule formation and proliferation of HMECs were profoundly augmented by siPTEN #1 and siSPRY1 #1 compared to the control siRNA group, similar to that observed in UCB-Exos treatment group (**Fig. 8B-F**). Taken together, our *in vitro* functional assays on HMECs suggest that inhibition of PTEN and SPRY1 via miR-21-3p mediates the pro-angiogenic effects of UCB-Exos on endothelial cells.

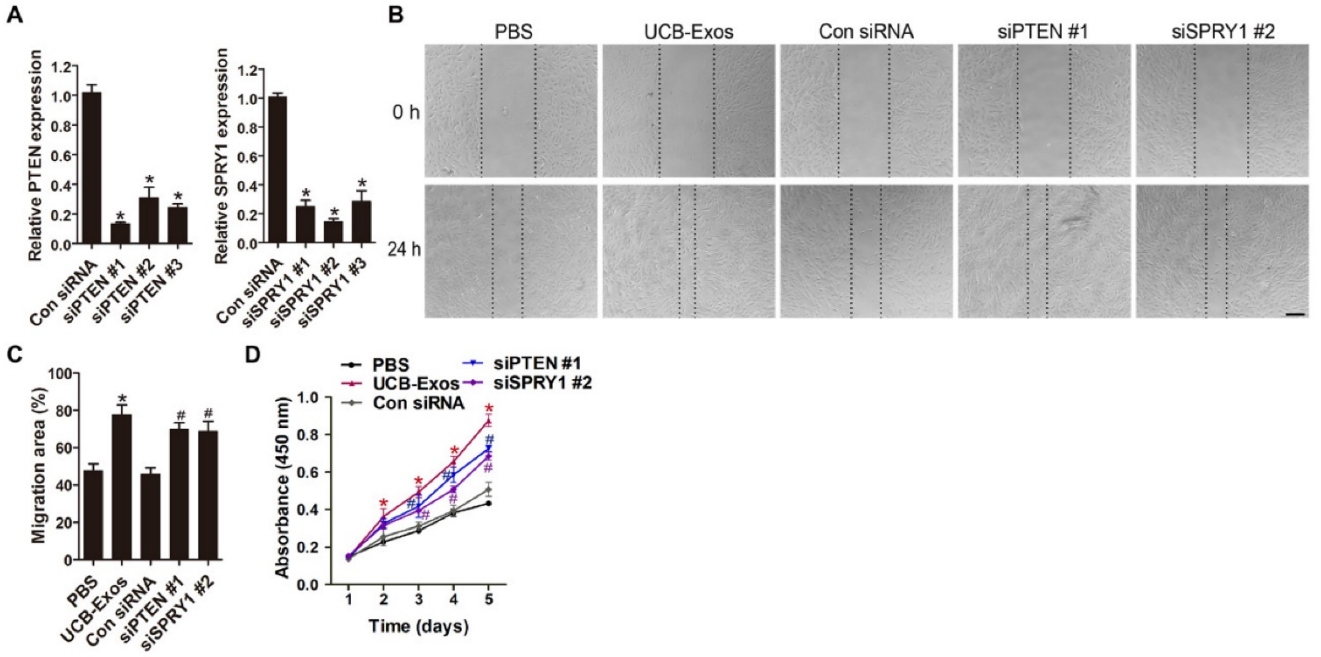

Figure 6. Inhibition of PTEN and SPRY1 induces UCB-Exos-like positive effects on fibroblast function. (A) The inhibitory efficiency of the siRNAs targeting PTEN and SPRY1 was verified by qRT-PCR. n = 3 per group. **(B)** The migration of HSFs in different treatment groups was tested by the scratch wound assay. **(C)** Quantitative analysis of the migration rates in (B). n = 3 per group. **(D)** CCK-8 analysis of HSFs proliferation in different treatment groups. n = 4 per group. **P* < 0.05 compared with the PBS group, # *P* < 0.05 compared with the control (Con) siRNA group.

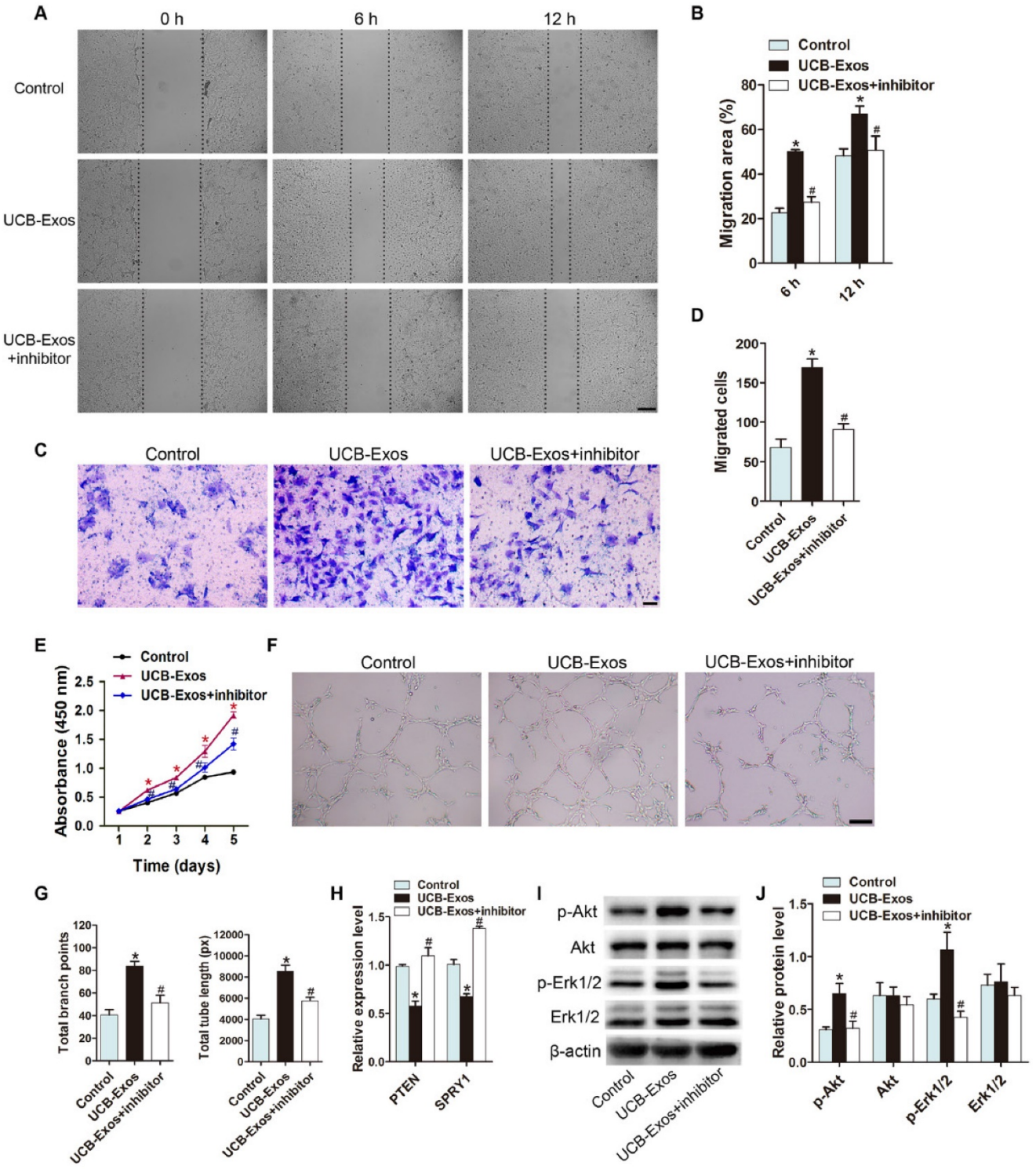

Figure 7. MiR-21-3p mediates the pro-angiogenic effects of UCB-Exos on endothelial cells. UCB-Exos induced a significant increase in the motility of HMECs, but the pro-migratory effect was decreased by the miR-21-3p inhibitor, as analyzed by the scratch wound assay **(A-B)** (Scale bar: 250 μm) and the transwell assay **(C-D)** (Scale bar: 100 μm). n = 3 per group. **(E)** The proliferation of HMECs receiving different treatments was assessed by CCK-8 analysis. n = 4 per group. **(F)** UCB-Exos increased the tube formation ability of HMECs, but this effect was decreased by miR-21-3p inhibition. Scale bar: 100 μm. **(G)** Quantitative analysis of the total branching points and total tube length in (F). n = 3 per group. **(H)** Detection of the expression of PTEN and SPRY1 by qRT-PCR analysis. n = 3 per group. **(I)** Detection of the phosphorylation levels of Akt and Erk1/2 by western blotting. n = 4 per group. *$P < 0.05$ compared with the control (Con) siRNA group, #$P < 0.05$ compared with the UCB-Exos (100 μg/mL) group.

Discussion

In this study, we provided the first demonstration that the local transplantation of UCB-Exos into mouse skin wounds induced prominent regenerative effects in the wound sites, as defined by more rapid wound closure and collagen deposition, higher rates of re-epithelialization and

new blood vessel formation, as well as less scar formation. We also demonstrated *in vitro* that UCB-Exos could be internalized into fibroblasts and endothelial cells, activate PI3K/Akt and ERK1/2 signaling, and enhance their functional properties by transferring miR-21-3p. Our results suggest that UCB-Exos may deliver miR-21-3p into resident fibroblasts and endothelial cells to evoke their regenerative responses, thereby accelerating cutaneous wound repair and regeneration.

In recent years, the application of plasma for tissue engineering is receiving great attention among scientists and clinicians [22-24]. In particular, platelet-rich plasma (PRP) has shown promising experimental and clinical results in soft tissue wound repair [23, 24]. Exosomes are critical paracrine mediators released by most cells and can be obtained from biological fluids including plasma. Recent studies have showed that the plasma-derived exosomes can serve as potential diagnostic biomarkers for various diseases [25], whereas few studies have used the whole blood plasma to isolate exosomes for tissue regeneration. A recent study by Guo et al reported that the exosomes derived from human peripheral blood PRP could exert beneficial effects on diabetic wound healing in rats [26], suggesting that exosomes are important effectors of PRP activity. However, it is noteworthy that PRP is a concentration of platelets in a small volume of plasma, and most of the supernatant plasma which may contain a large amount of exosomes is discarded during harvest procedures of PRP [23, 24, 26]. Indeed, the exosomes derived from PRP are mainly released from the platelets activated by calcium and thrombin [26]. It remains unclear whether exosomes naturally existing in the plasma can induce tissue repair and regeneration. Herein, we collected exosomes from human UCB plasma and confirmed their pro-regenerative effects on wound healing, indicating that exosomes are important mediators of plasma function and can be utilized as a novel therapeutic nano-delivery system for wound healing.

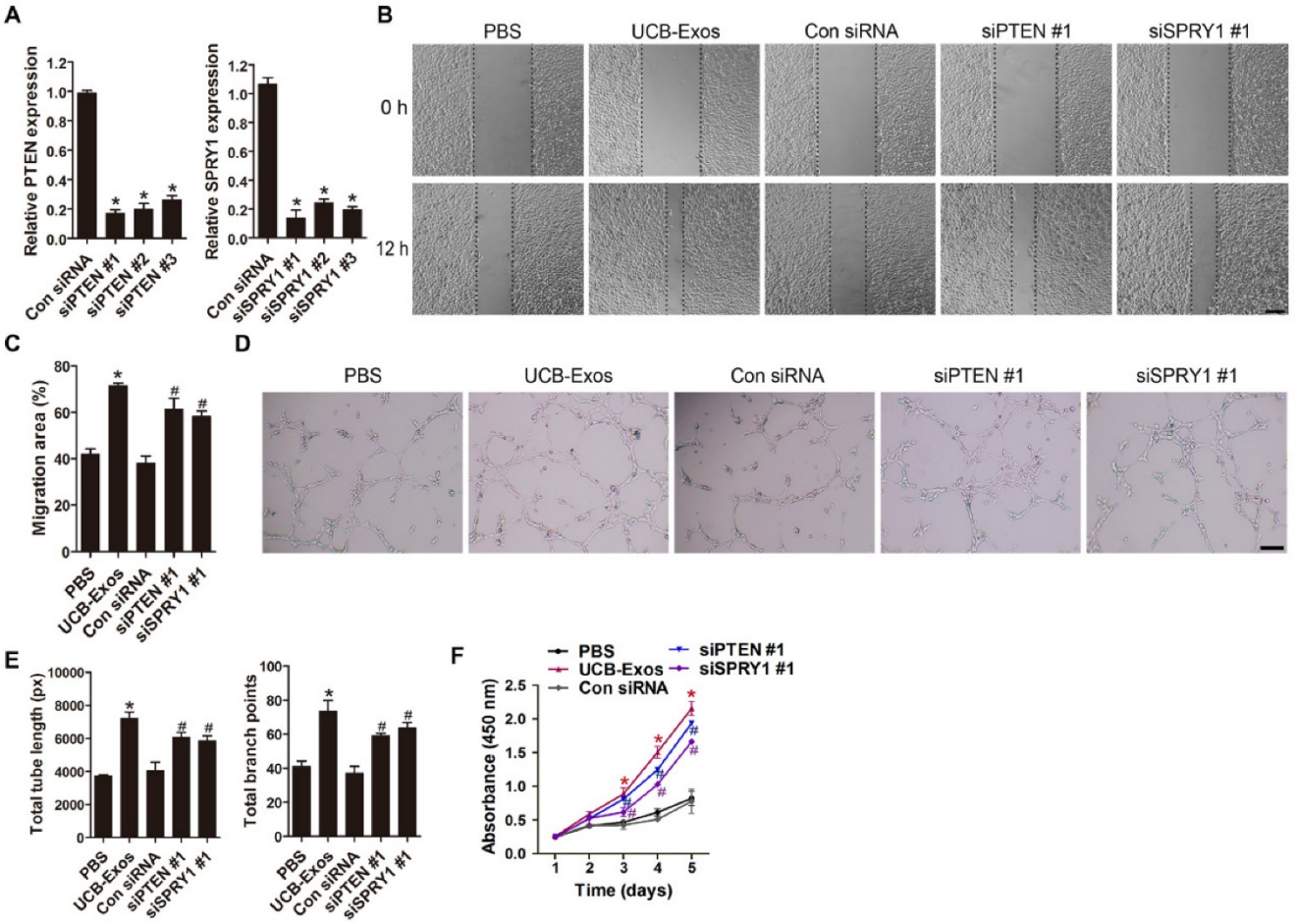

Figure 8. Inhibition of PTEN and SPRY1 induces UCB-Exos-like pro-angiogenic effects on endothelial cells. (A) The inhibitory efficiency of the siRNAs targeting PTEN and SPRY1 was verified by qRT-PCR. n = 3 per group. **(B)** The migration of HMECs in different treatment groups was tested by the scratch wound assay. **(C)** Quantitative analysis of the migration rates in (B). n = 3 per group. **(D-E)** Representative images and quantification of HMECs tube formation in different treatment groups. n = 3 per group. **(F)** CCK-8 analysis of HMECs proliferation in different treatment groups. n = 4 per group. **P* < 0.05 compared with the PBS group, # *P* < 0.05 compared with the Con siRNA group.

Fibroblasts are the major effector cells in the wound healing of soft tissue. Their proliferation and migration are essential for wound contraction, collagen synthesis and tissue remodeling [27]. In this study, we evaluated the effects of UCB-Exos on the behavior of fibroblasts *in vitro*. The results revealed that these nanoparticles could be internalized by fibroblasts and significantly enhance their proliferation and migration, suggesting that the activation of fibroblasts is a mechanism through which UCB-Exos stimulate wound healing. New blood vessels formation in postnatal life occurs mainly via angiogenesis, which provides oxygen and nutrients to the wound for sustaining fibroblast proliferation, collagen synthesis, and re-epithelialization [11]. The results of our study showed that UCB-Exos transplantation profoundly increased the number of newly formed blood vessels in the wound areas, suggesting that UCB-Exos treatment augment the angiogenic responses in the wound sites. Using a series of *in vitro* angiogenesis-related assays, we found that UCB-Exos could markedly enhance the migration, proliferation, and angiogenic tubule formation of endothelial cells, which further confirmed the pro-angiogenic property of UCB-Exos. Thus, the beneficial effects of UCB-Exos on wound healing may be mainly attributed to their function in promotion of endogenous fibroblasts and endothelial cells.

MiRNAs are a class of 20-24 nt small non-coding RNAs that function as inhibitors of target gene expression by inducing mRNA degradation or translational repression [28]. MiR-21 is one of the most well studied miRNAs and is implicated in preventing invasion of cancer cells in many types of cancer, including skin cancers [29]. MiR-21 expression was found to be up-regulated after skin injury and could promote keratinocyte migration to accelerate reepithelialization of skin wounds [17]. Inhibition of miR-21 could result in a significant delay of wound closure with less fibroblasts and collagen deposition in the wound sites, suggesting that miR-21 is a positive modulator of fibroblast function [17]. Although few studies have deciphered the role of miR-21 in wound revascularization, the beneficial effects of miR-21 on endothelial cell function and tumor angiogenesis have been evaluated [18, 21]. These findings reveal that miR-21 up-regulation may facilitate wound healing.

It has been shown that exosomes contain large amounts of miRNAs and can serve as vehicles to transfer miRNAs to recipient cells, where the exogenous miRNAs can alter the gene expression and bioactivity of recipient cells [28]. MiR-21 has been identified in exosomes derived from cancer-associated adipocytes and fibroblasts [28], bronchial epithelial cells [18], dendritic cells [30], and serum samples from patients with laryngeal cancer [31]. Here, we detected high level of miR-21-3p, but not miR-21-5p, in UCB-Exos. After incubating with UCB-Exos for a very short period of time (3 h), we found that miR-21-3p expression was remarkably enhanced in fibroblasts and endothelial cells, indicating that miR-21-3p can be transferred from UCB-Exos to recipient cells. Studies have demonstrated that the miR-21-dependent regulation of fibroblasts' and endothelial cells' activities is mediated by the activation of PI3K/Akt and ERK1/2 signaling through downregulation of PTEN and SPRY1 [19-21]. In accord with these published findings, results of our study showed that the expression levels of PTEN and SPRY1 were significantly decreased, whereas the activities of PI3K/Akt and ERK1/2 signaling was markedly augmented in fibroblasts and endothelial cells stimulated by the miR-21-3p-contaning UCB-Exos. However, these effects induced by UCB-Exos were notably reversed by the specific inhibitor targeting miR-21-3p. In addition, we found that the UCB-Exos-induced promotion of fibroblast function and angiogenesis of endothelial cells was also attenuated, but not entirely abolished, by miR-21-3p inhibition. We also found that knocking down the expression of miR-21 target genes PTEN and SPRY1 could achieve UCB-Exos-like, but not all, positive effects on fibroblast function and endothelial angiogenesis. These findings suggest that miR-21-3p is one of the critical mediators in UCB-Exos-induced regulation of characteristics of fibroblasts and endothelial cells by targeting PTEN and SPRY1, and other signaling molecules may also be involved in this process, which warrants further investigation. Another limitation of our study is that no *in vivo* data directly show the role of miR-21-3p in UCB-Exos-induced regulation of wound healing.

In this work, we traced the administrated UCB-Exos in skin tissues at different time point and found the accumulation of PKH67-labeled UCB-Exos in skin tissues at 3 h after injection. Although UCB-Exos were still present at 2 days after injection, the density had been markedly reduced. 3 days after injection, the signal disappeared. These data, along with the *in vivo* and *in vitro* results obtained in our study, suggest that a single dose injection of UCB-Exos may provide instant but strong stimuli to the resident skin cells, where the exogenous miR-21-3p transferred from UCB-Exos alters the expression of target genes and activates the regenerative responses of skin cells, which finally cause a significant acceleration of the wound healing process.

There were a number of limitations in the present study. First, it remains to be determined whether sustained delivery of UCB-Exos can induce similar or much better pro-regenerative effects in skin wounds in mice. Moreover, the changes in expression of miR-21-3p in wound tissues after UCB-Exos transplantation and the precise mechanism by which miR-21-3p regulates the expression of target genes were not further evaluated in the present study. In addition, although we used exosomes from 3 different donors-derived UCB for *in vitro* assays, we just used exosomes from a single donor-derived UCB for verifying their functional properties *in vivo*.

In summary, our results show that UCB-Exos can effectively enhance cutaneous wound healing in mice and the underlying mechanism may be their activation of function properties of fibroblasts and endothelial cells in the wounds, as UCB-Exos can enhance the proliferation and migration of fibroblasts, as well as the angiogenic activities of endothelial cells *in vitro*. In the UCB-Exos-dependent regulation of fibroblast function and endothelial angiogenesis, miR-21-3p plays a crucial role since suppression of miR-21-3p can markedly reduce the regulatory effects of UCB-Exos. Our findings suggest that UCB-Exos may represent a novel therapeutic tool for soft tissue wound healing.

Abbreviations

UCB: umbilical cord blood; UCB-Exos: exosomes from human umbilical cord blood plasma; PTEN: phosphatase and tensin homolog; SPRY1: sprouty homolog 1; miRNA: microRNA; mRNA: messenger RNA; DLS: dynamic light scattering; TEM: transmission electron microscope; TSG101: tumor susceptibility gene 101; H&E: hematoxylin and eosin; HSFs: human skin fibroblasts; HMECs: human microvascular endothelial cells; CCK-8: cell counting kit-8; qRT-PCR: quantitative real-time PCR; siRNAs: small interfering RNA; SDS-PAGE: sodium dodecyl sulfate-polyacrylamide gel electrophoresis; PI3K: phosphoinositide 3-kinase; p-Akt: phosphorylate Akt; Erk: extracellular signal regulated kinase; p-Erk: phosphorylate Erk; PRP: platelet-rich plasma.

Acknowledgements

This work was supported by the Thousand Youth Talents Plan of China (**Grant No. D1119003**), the Excellent Young Scientist Award of National Natural Science Foundation of China (**Grant No. 81522012**), the National Natural Science Foundation of China (**Grant No. 81670807, 81702237, 81600699),** the Youth Foundation of Xiangya Hospital in Central South University (**Grant No. 2016Q10**), the Fundamental Research Funds for the Central Universities of Central South University (**Grant No. 2017zzts014, 2017zzts032**), Hunan Province Natural Science Foundation of China (**Grant No. 2017JJ3501**), and China Postdoctoral Science Foundation (**Grant No.** 2017M612596). We thank Yue-Lan Liu, Wen-Yan Jian and Kui-Lin Fei for their assistance in the collection of the human UCB samples.

Author Contributions

HX and CYC conceived and designed the experiments. YH, SSR and CYC performed the experiments. HX, CYC and YH wrote the manuscript. YH and CYC analysed the data and prepared all the figures. YJT, JL and HML helped with the biochemical experiment. ZXW, JC and WSZ provided technical support. All authors reviewed and agreed the manuscript.

Supplementary Material

Supplementary figure S1 and methods.
http://www.thno.org/v08p0169s1.pdf

Competing Interests

The authors have declared that no competing interest exists.

References

1. van Zanten MC, Mistry RM, Suami H, Campbell-Lloyd A, Finkemeyer JP, Piller NB, et al. The Lymphatic Response to Injury with Soft-Tissue Reconstruction in High-Energy Open Tibial Fractures of the Lower Extremity. Plast Reconstr Surg. 2017; 139: 483-91.
2. Bhandari M, Petrisor BA, Jeray KJ. Wound Irrigation in Initial Management of Open Fractures. N Engl J Med. 2016; 374: 1789-90.
3. Falanga V. Wound healing and its impairment in the diabetic foot. Lancet. 2005; 366: 1736-43.
4. Plikus MV, Guerrero-Juarez CF, Ito M, Li YR, Dedhia PH, Zheng Y, et al. Regeneration of fat cells from myofibroblasts during wound healing. Science. 2017; 355: 748-52.
5. Doi H, Kitajima Y, Luo L, Yan C, Tateishi S, Ono Y, et al. Potency of umbilical cord blood- and Wharton's jelly-derived mesenchymal stem cells for scarless wound healing. Sci Rep. 2016; 6: 18844.
6. He B, Li X, Yu H, Zhou Z. Therapeutic potential of umbilical cord blood cells for type 1 diabetes mellitus. J Diabetes. 2015; 7: 762-73.
7. Amariglio N, Hirshberg A, Scheithauer BW, Cohen Y, Loewenthal R, Trakhtenbrot L, et al. Donor-derived brain tumor following neural stem cell transplantation in an ataxia telangiectasia patient. PLoS Med. 2009; 6: e1000029.
8. Kansu E. Thrombosis in stem cell transplantation. Hematology. 2012; 17 Suppl 1: S159-62.
9. Herberts CA, Kwa MS, Hermsen HP. Risk factors in the development of stem cell therapy. J Transl Med. 2011; 9: 29.
10. Tkach M, Thery C. Communication by Extracellular Vesicles: Where We Are and Where We Need to Go. Cell. 2016; 164: 1226-32.
11. Zhang J, Chen C, Hu B, Niu X, Liu X, Zhang G, et al. Exosomes Derived from Human Endothelial Progenitor Cells Accelerate Cutaneous Wound Healing by Promoting Angiogenesis Through Erk1/2 Signaling. Int J Biol Sci. 2016; 12: 1472-87.
12. Basu J, Ludlow JW. Exosomes for repair, regeneration and rejuvenation. Expert Opin Biol Ther. 2016: 1-18.
13. Zhang B, Wang M, Gong A, Zhang X, Wu X, Zhu Y, et al. HucMSC-Exosome Mediated-Wnt4 Signaling Is Required for Cutaneous Wound Healing. Stem cells. 2015; 33: 2158-68.
14. Jia R, Li J, Rui C, Ji H, Ding H, Lu Y, et al. Comparative Proteomic Profile of the Human Umbilical Cord Blood Exosomes between Normal and Preeclampsia Pregnancies with High-Resolution Mass Spectrometry. Cell Physiol Biochem. 2015; 36: 2299-306.
15. van Balkom BW, de Jong OG, Smits M, Brummelman J, den Ouden K, de Bree PM, et al. Endothelial cells require miR-214 to secrete exosomes that suppress senescence and induce angiogenesis in human and mouse endothelial cells. Blood. 2013; 121: 3997-4006, S1-15.

16. Madhyastha R, Madhyastha H, Nakajima Y, Omura S, Maruyama M. MicroRNA signature in diabetic wound healing: promotive role of miR-21 in fibroblast migration. Int Wound J. 2012; 9: 355-61.
17. Wang T, Feng Y, Sun H, Zhang L, Hao L, Shi C, et al. miR-21 regulates skin wound healing by targeting multiple aspects of the healing process. Am J Pathol. 2012; 181: 1911-20.
18. Liu Y, Luo F, Wang B, Li H, Xu Y, Liu X, et al. STAT3-regulated exosomal miR-21 promotes angiogenesis and is involved in neoplastic processes of transformed human bronchial epithelial cells. Cancer Lett. 2016; 370: 125-35.
19. Thum T, Gross C, Fiedler J, Fischer T, Kissler S, Bussen M, et al. MicroRNA-21 contributes to myocardial disease by stimulating MAP kinase signalling in fibroblasts. Nature. 2008; 456: 980-4.
20. Zhu HY, Li C, Bai WD, Su LL, Liu JQ, Li Y, et al. MicroRNA-21 regulates hTERT via PTEN in hypertrophic scar fibroblasts. PloS one. 2014; 9: e97114.
21. Liu LZ, Li C, Chen Q, Jing Y, Carpenter R, Jiang Y, et al. MiR-21 induced angiogenesis through AKT and ERK activation and HIF-1alpha expression. PloS one. 2011; 6: e19139.
22. Villeda SA, Plambeck KE, Middeldorp J, Castellano JM, Mosher KI, Luo J, et al. Young blood reverses age-related impairments in cognitive function and synaptic plasticity in mice. Nat Med. 2014; 20: 659-63.
23. Nishimoto S, Kawai K, Tsumano T, Fukuda K, Fujiwara T, Kakibuchi M. Impacts of bone marrow aspirate and peripheral blood derived platelet-rich plasma on the wound healing in chronic ischaemic limb. J Plast Surg Hand Surg. 2013; 47: 169-74.
24. Spyridakis M, Christodoulidis G, Chatzitheofilou C, Symeonidis D, Tepetes K. The role of the platelet-rich plasma in accelerating the wound-healing process and recovery in patients being operated for pilonidal sinus disease: preliminary results. World J Surg. 2009; 33: 1764-9.
25. Sodar BW, Kittel A, Paloczi K, Vukman KV, Osteikoetxea X, Szabo-Taylor K, et al. Low-density lipoprotein mimics blood plasma-derived exosomes and microvesicles during isolation and detection. Sci Rep. 2016; 6: 24316.
26. Guo SC, Tao SC, Yin WJ, Qi X, Yuan T, Zhang CQ. Exosomes derived from platelet-rich plasma promote the re-epithelization of chronic cutaneous wounds via activation of YAP in a diabetic rat model. Theranostics. 2017; 7: 81-96.
27. Driskell RR, Lichtenberger BM, Hoste E, Kretzschmar K, Simons BD, Charalambous M, et al. Distinct fibroblast lineages determine dermal architecture in skin development and repair. Nature. 2013; 504: 277-81.
28. Au Yeung CL, Co NN, Tsuruga T, Yeung TL, Kwan SY, Leung CS, et al. Exosomal transfer of stroma-derived miR21 confers paclitaxel resistance in ovarian cancer cells through targeting APAF1. Nat Commun. 2016; 7: 11150.
29. Pfeffer SR, Yang CH, Pfeffer LM. The Role of miR-21 in Cancer. Drug Dev Res. 2015; 76: 270-7.
30. Mittelbrunn M, Gutierrez-Vazquez C, Villarroya-Beltri C, Gonzalez S, Sanchez-Cabo F, Gonzalez MA, et al. Unidirectional transfer of microRNA-loaded exosomes from T cells to antigen-presenting cells. Nat Commun. 2011; 2: 282.
31. Wang J, Zhou Y, Lu J, Sun Y, Xiao H, Liu M, et al. Combined detection of serum exosomal miR-21 and HOTAIR as diagnostic and prognostic biomarkers for laryngeal squamous cell carcinoma. Med Oncol. 2014; 31: 148.